# A debonding model for superficial reinforcements under inclined loading

(Article begins on next page)

07 July 2024

# A debonding model for superficial reinforcements under inclined loading

Laura De Lorenzis, Giorgio Zavarise
*Department of Innovation Engineering, University of Salento, Italy*
*Via per Monteroni, Ed. Stecca, 73100 Lecce*
*E-mail*: *laura.delorenzis@unile.it*
*E-mail*: *giorgio.zavarise@unile.it*

SUMMARY: This paper presents a numerical model of the interface between a quasi-brittle substrate and a thin elastic adherend subjected to mixed-mode loading. The interface is modeled by zero-thickness contact elements, which describe both debonding and contact within a unified framework using the node-to-segment contact strategy. Uncoupled cohesive interface constitutive laws are adopted in the normal and tangential directions. The formulation is implemented and tested using the finite element code FEAP. The model is able to predict the response of the bonded joint as a function of the main parameters, which are identified through dimensional analysis. The main objective is to compute the debonding load and the effective bond length of the adherend, i.e. the value of bond length beyond which a further increase of bond length has no effect on the debonding load, as functions of the peel angle.

## 1. INTRODUCTION

The mechanics of interfacial bond between a thin plate and a flat quasi-brittle substrate under mode-II loading has been extensively studied both with experiments and theories based on analytical and numerical methods (Taljsten 1996, De Lorenzis et al. 2001, Yuan et al. 2004, Ferracuti et al. 2006, among others). These investigations have clarified the whole range of response of a bonded joint subjected to predominant shear stresses, from the linear elastic stage up to the final debonding. For thin plates bonded by high-strength adhesives to quasi-brittle substrates, debonding failure typically occurs by cohesive mode-II fracture of the substrate, where mode II is intended in a macroscopic sense. A typical example is given by fiber-reinforced polymer (FRP) strips bonded to concrete or masonry.

Mixed-mode conditions take place at a variety of bonded interfaces existing in practice, such as in various types of lap joints (Kafkalidis and Thouless 2002), and at the interface between FRP and substrate in the proximity of inclined cracks or at the edge of the FRP plate (Yao et al., 2005, Pan and Leung, 2006, Bruno et al. 2007). Mode mixity also affects interfacial debonding between a thin plate and a curved substrate, which is relevant to the structural analysis of beams with curved soffit or arches strengthened with thin bonded plates (De Lorenzis et al. 2006).

The so-called peel-test has been widely used to characterize the bond behaviour of adhesives (Bikerman 1957, Williams 1997). In this test a thin plate bonded to a substrate is pulled from it at a certain angle (the "peel angle") and the "peel force" needed to produce

debonding is measured. In this configuration the interface is subjected to shear and normal stresses, hence debonding occurs by mixed-mode fracture. However, as large peel angles (>20°) are typically considered, mode I is largely dominant and a global energy balance involving a single value of fracture energy is used. In cases where debonding is controlled by cohesive failure within the adhesive, the test can be used to evaluate the fracture energy of adhesives. In the most general case failure involves the weakest link between the adhesive, the substrate and the bond line, or even a combination of them (Bastianini 2003, Karbhari et al. 1997). Hence the resulting fracture energy is that of the interface intended in a general sense.

Several elastic analyses of the peel test have been presented in the early literature on the subject (Bikerman 1957, among many others), up to the recent analytical solution proposed by Yuan et al. (2007). Other authors have investigated the interfacial stress distributions with finite element analyses (e.g. Kim and Aravas 1988). These studies showed that interfacial shear and normal stresses are highly localized in the vicinity of the loaded end. Also, as the peel angle is different from zero, the magnitude of the interfacial normal stresses can be very significant compared with that of the interfacial shear stress at the loaded end. Other studies have focused on the effects of plasticity in the adherend (Crocombe and Adams, 1982, Kim and Aravas 1988, Aravas et al. 1989, Wei and Hutchinson 1998).

After an initial focus on stress-based debonding criteria, experiments have shown that energy-based criteria are more appropriate for the determination of the interfacial fracture strength. Hence, some authors have studied the mechanics of the peel test using linear-elastic and non-linear fracture mechanics (Williams 1997, Kim and Aravas 1988, Aravas et al. 1989). In particular, Wei and Hutchinson (1998) adopted the cohesive zone modelling approach, mainly focusing on the role of interface strength and the plastic energy dissipated in elasto-plastic adherends. They used coupled cohesive laws obtained from a potential, yielding the same fracture energy regardless of the mode mixity. On the other hand, the range of peel angles considered in the study implied a predominance of mode-I conditions.

Few studies have addressed the bond of linearly elastic adherends to quasi-brittle substrates under inclined loading. Karbhari et al. (1997) developed a peel test to investigate the bond behaviour between FRP strips and concrete and discussed different mechanisms of interfacial fracture. Dai et al. (2004) studied mixed-mode fracture at the FRP-concrete interface by using a specially designed beam test setup. They observed that the effective bond length, i.e. the value of bond length beyond which a further increase of bond length produces no increase in the debonding load, is shorter for interfaces under inclined loading than under mode-II loading. They also found that the peeling force that the interface can resist is rather low. Finally, they determined a mixed mode energy envelope governing interfacial fracture. Yao et al. (2005) conducted experiments on FRP-concrete bonded joints, including a few tests where the FRP was subjected to inclined loading with a small inclination angle (1.7°). They observed a relatively limited detrimental effect of this angle on the bond strength. Pan and Leung (2007) developed a test setup to investigate FRP-concrete bond under mixed mode conditions, and found a significant effect of the mode-I component on the debonding load. They also presented a simple analytical model.

Clearly, numerical modelling is needed to more deeply understand the behaviour of the interface between a thin elastic adherend and a quasi-brittle substrate subjected to inclined loading. As mentioned earlier, modelling of the peel test in the literature has focused on cases

of mode-I dominance, where the use of a global energy balance involving mode-I fracture energy is well justified. However, if the peel angle is small, such as in the case of debonding along inclined cracks or from a substrate with a large radius of curvature, mode mixity cannot be neglected. Finally, a numerical estimate of the effective bond length under mixed mode loading is also of significance and has not been carried out in previous studies.

This paper presents a numerical model of the interface between a quasi-brittle substrate and a thin elastic adherend subjected to inclined loading. The interface is modelled by zero-thickness contact elements, using the node-to-segment strategy and describing decohesion and contact within a unified framework. The formulation is implemented and tested using the finite element code FEAP (courtesy of Prof. R.L. Taylor). The main objective of the model is to compute the debonding load of the adherend and its effective bond length as functions of the peel angle, in order to evaluate the effect of mode mixity on the macroscopic interfacial strength. Numerical tests are performed with a simple peel test model to predict the response of the bonded joint as a function of the main parameters, which are identified through dimensional analysis. Beside its significance to understand the effect of mixed-mode conditions on debonding, the study of the peel test can be considered a preliminary step to the study of a curved interface, regarding the latter as an interface subjected to a variable peel angle.

## 2. MECHANICS OF THE PEEL TEST

Consider a thin plate of thickness $t$ and width $b$, made of a linearly elastic material with elastic modulus $E$, bonded to a flat rigid substrate, and loaded with a force $F$ at an angle $\theta$ from the horizontal. An energy balance can be used to relate the experimentally determined peel force (corresponding to steady-state peeling) to the specific fracture energy. The energy release rate $G$ can be expressed as follows (Williams, 1997)

$$G = \frac{F}{b}\left(1 - \cos\theta + \frac{F}{2Ebt}\right) \tag{1}$$

Assuming that the work of separation (or fracture energy) has the same value $G_f$ regardless of the combination of normal and tangential displacements taking place in the separation of the interface, the critical condition is reached when $G = G_f$ and the steady-state peeling load $F_{peel}$ is easily derived

$$\frac{F_{peel}}{b} = \sqrt{E^2 t^2 \left(1 - \cos\theta\right)^2 + 2EtG_f} - Et\left(1 - \cos\theta\right) \tag{2}$$

For a peel angle equal to zero, Eq. (2) reduces to the well-known expression for the mode-II debonding load of a thin plate bonded to a rigid substrate (Taljsten 1996). Clearly, $G_f$ in the equations above corresponds to the fracture energy of the adhesive, of the substrate, or of the interface, depending on whether the debonding path is, respectively, within the adhesive, within the substrate, or along the bond line. Note that the assumption of equal $G_f$ regardless of the mode mixity is not realistic, as many tests have shown that the mode-II fracture energy is larger

than the mode-I value. Hence Eq. (2) is expected to be valid with $G_f = G_{If}$ for large peel angles, i.e. in mode-I dominance, and with $G_f = G_{IIf}$ for small peel angles, i.e in mode-II dominance. $G_{If}$ and $G_{IIf}$ denote mode-I and mode-II fracture energies, respectively.

### 3. INTERFACE MODELING
#### 3.1. Possible approaches for cohesive zone modelling in mixed-mode conditions

Due to its simplicity, cohesive zone modelling is largely used for a variety of applications, including fracture of ductile and brittle solids, delamination in composites at the micro- or macro-scale, and behaviour of adhesive layers. Different approaches have been used in the literature for cohesive zone modelling of interfaces under mixed-mode conditions:

1. *Uncoupled cohesive zone modelling.* In this approach, cohesive laws in the normal and tangential directions are independent from each other. This approach was used by Kafkalidis and Thouless (2002), and Li et al. (2006), among others. The energy release rates in mode I ($G_I$) and mode II ($G_{II}$) are identified as the areas under the respective cohesive laws. The total energy release rate is the sum of $G_I$ and $G_{II}$. A further distinction can be made between approaches in which:
   a. A mixed-mode fracture criterion is introduced, see e.g. Kafkalidis and Thouless (2002), and Li et al. (2006). Once the failure condition is reached, the element is considered no longer capable to bear any load. This assumption yields sudden drops in the tractions before the critical separation is reached. Nevertheless, this approach was shown to provide good capabilities to capture essential properties of adhesive joints.
   b. No mixed-mode fracture criterion is introduced. In this case, failure is assumed when either $G_I$ or $G_{II}$ reach their respective maximum values.
2. *Coupled cohesive zone modelling.* In this approach, cohesive laws in the normal and tangential directions are linked to each other, typically by means of a coupling parameter. Also in this case a further distinction can be made between approaches in which:
   a. The cohesive laws are derived from a potential. A frequently used coupled cohesive law of this type is that developed by Tvergaard (1990), which uses a dimensionless coupling parameter between the normal and tangential laws. With this approach, the fracture energy is the same in all mode mixities. This is often regarded as a drawback, as the experimental evidence indicates the fracture energy to be often significantly larger in mode II than in mode I (Hogberg 2006).
   b. The cohesive laws are not derived from a potential. Laws of this type have been proposed by Xu and Needleman (1993), and Hogberg (2006), among others. These laws allow for different fracture energies in different mode mixities. Also, the lack of a potential introduces a path-dependency, which is in fact physical considering that cohesive zone models can describe an irreversible damage process at an interface (van den Bosch et al. 2006).

#### 3.2. Interface constitutive laws and finite element formulation

In this paper uncoupled cohesive laws are adopted both in the normal and tangential directions. Tension relates the normal relative displacement, $g_N > 0$, and the normal stress,

$p_N$, while shear relates the tangential relative displacement, $g_T$, and the tangential stress, $p_T$. This choice is made to enable the use of different values for the mode-I and mode-II interfacial fracture energies, in agreement with the experimental evidence. In the normal direction under compression the non-penetration condition is enforced using the penalty method.

The cohesive laws are taken as bilinear (Figure 1). This simple shape is able to capture the three characteristic parameters of the interface, i.e. the fracture energies (areas underneath the curves), the cohesive strengths, $p_{N\max}$ and $p_{T\max}$, and the linear elastic properties (slopes of the curves in the ascending branch). For this reason it is often used to model the interfacial behaviour of FRP bonded to quasi-brittle substrates (Yuan et al. 2004). Following the approach in Kafkalidis and Thouless (2002), the energy release rates in mode I and mode II are identified as the areas under the respective cohesive laws integrated up to the current values of $g_N$ and $g_T$, and the simplest possible mixed-mode failure criterion is assumed as

$$\frac{G_I}{G_{If}} + \frac{G_{II}}{G_{IIf}} = 1 \tag{3}$$

Once the failure criterion is met for an element in the cohesive zone, the element is assumed to be no longer capable to bear any load. The mode-mixity can be estimated directly from the numerical predictions by examining the value of $G_{II}/G_I$ for a crack-tip cohesive zone element just before it fails.

The above contact and cohesive models have been implemented into a contact element based on the node-to-segment strategy as employed in Wriggers et al. (1998) and generalized to handle cohesive forces in both the normal and tangential directions. Depending on the contact status, an automatic switching procedure is used to choose between cohesive and contact models. Each element contribution for the cohesive and contact forces is suitably added to the global virtual work equation as

$$\delta W = F_N \delta g_N + F_T \delta g_T \tag{4}$$

where $F_N$ and $F_T$ denote, respectively, the normal and tangential force.
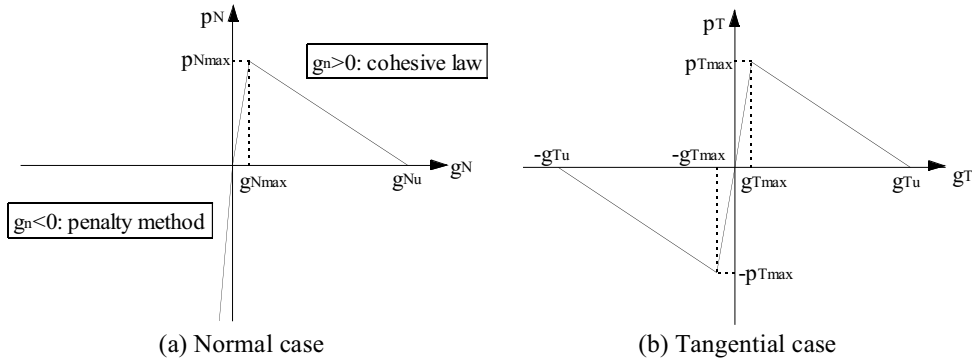


(a) Normal case  (b) Tangential case

Figure 1. Relationships between interfacial tractions and relative displacements.

The adherend is modelled with two-dimensional, finite deformation, linearly-elastic beam elements, whereas the substrate is discretized with 4-node isoparametric plane stress elastic elements. The substrate elements are given a very large elastic modulus in order to minimize the effects of the substrate compliance on results. The non-linear problem, depicted in Figure 2, is solved with a Newton-Raphson procedure. The global tangent stiffness matrix is obtained with a consistent linearization of all the contributions given by (4). The discretization is refined appropriately to yield mesh-independent results. The model is implemented in the finite element code FEAP.
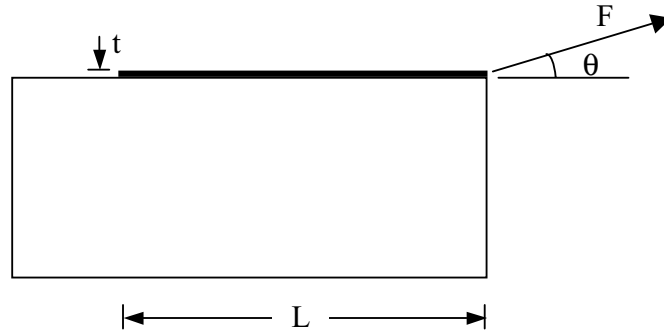


Figure 2. Scheme of the problem.

### 3.3. Dimensional analysis and reference values of the parameters

By means of dimensional analysis, the steady-state peeling load can be expressed as follows:

$$\frac{F_{peel}}{p_{T\max}L} = f\left(\frac{Et}{G_{If}}, \frac{L}{t}, \frac{G_{IIf}}{G_{If}}, \frac{p_{N\max}}{E}, \frac{p_{T\max}}{p_{N\max}}, \theta\right) \tag{5}$$

where $L$ is the bond length. The above expression neglects the effect of the shape of the cohesive laws, which was shown to have a minor influence on predictions of cohesive zone models (Wei and Hutchinson 1998), and is herein kept constant. In this paper the attention is focused on the role of $\theta$, $L/t$ and $G_{IIf}/G_{If}$. The following reference values are adopted for the parameters involved in the problem: $G_{If} = 0.1\,N/mm$, $G_{IIf} = 0.4\,N/mm$, $p_{N\max} = 2\,MPa$, $p_{T\max} = 4\,MPa$, $E = 250\,GPa$, $t = 0.165\,mm$, $L = 100\,mm$.

The ultimate values of the normal and tangential relative displacements, $g_{Nu}$, $g_{Tu}$, follow from the above as $0.1\,mm$ and $0.2\,mm$, respectively. The $g_{N\max}/g_{Nu}$ and $g_{T\max}/g_{Tu}$ ratios, giving the shape of the cohesive laws, are assumed equal to $0.1$ in all analyses. The peel angle is varied between $0°$ and $10°$.

RESULTS

3.4. Effect of the peel angle

The load vs. displacement relationships given by the numerical model for different peel angles is shown in Figure 3-a. Both load and displacement refer to the direction given by the peel angle. The curves feature an ascending branch up to a peak value of force, followed by a plateau representing the steady-state peeling phase. The corresponding force is the steady-state peeling force, which can be significantly larger than the force at the onset of interfacial failure (Cui et al. 2003). Note that the shape of the force-displacement curve in the ascending portion and the presence itself of a peak before the steady-state peeling phase depend on the length of the unbonded portion of the adherend, which is equal to zero in the present case. However, such length does not affect the steady-state peeling load. The difference between peak and steady-state peeling loads is more pronounced for larger peel angles.

Figure 3-b shows that the normalized steady-state peeling load, $F_{peel}/p_{T\max}L$, decreases rapidly as the peel angle increases. The solid curves are obtained from Eq. (2) by substituting $G_f$ with $G_{If}$ and $G_{IIf}$, whereas the dots are predictions of the numerical model. Numerical results show a gradual transition from the mode-II curve to the mode-I curve as the peel angle increases, in accordance with the variation of the mode mixity at interface failure.



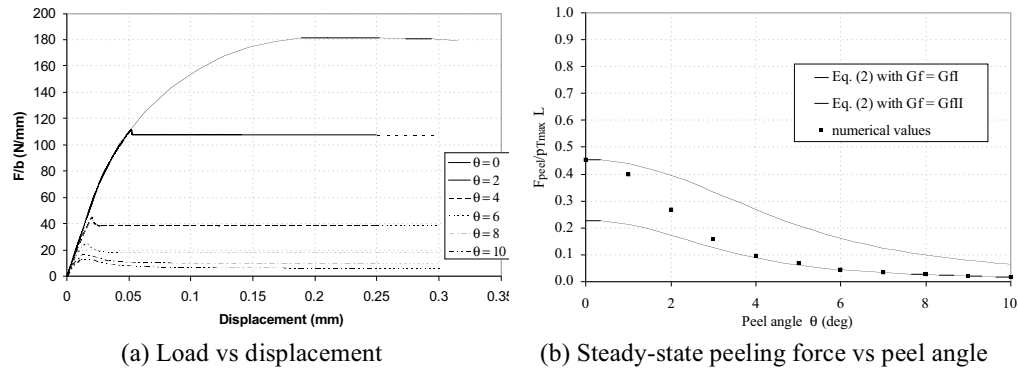(a) Load vs displacement      (b) Steady-state peeling force vs peel angle

Figure 3. Effect of the peel angle.

This variation can be further appreciated by looking at the interfacial stress distributions in Figures 4 through 6, where $x$ is the coordinate along the bond length. By extending to the mixed-mode case the terminology adopted by Yuan et al. (2004), the bonded joint is seen to move from an *elastic stage*, where normal and tangential stresses are within the first branch of the cohesive law along the entire bond length (Figures 4-a to 6-a), through an *elastic – softening stage*, where part of the bond length is subjected to interfacial stresses within the second branch of the cohesive law (Figures 4-b to 6-b), to an *elastic – softening – debonding stage*, where a portion of the bond length closest to the loaded end has debonded (Figures 4-c to 6-c). Due to the existence of two cohesive laws for the normal and tangential directions, intermediate situations can occur, where the interface is, e.g., at the elastic stage in the normal direction and already at the elastic–softening stage in the tangential direction, and so forth,

depending on the combination of the various parameters. However, the steady-state peeling phase invariably corresponds to the elastic–softening–debonding stage in both normal and tangential directions. In this phase, and in presence of a sufficiently long bond length, the interfacial stress profiles remain constant and translate from the loaded end to the free end of the joint as more and more contact elements sequentially reach failure.
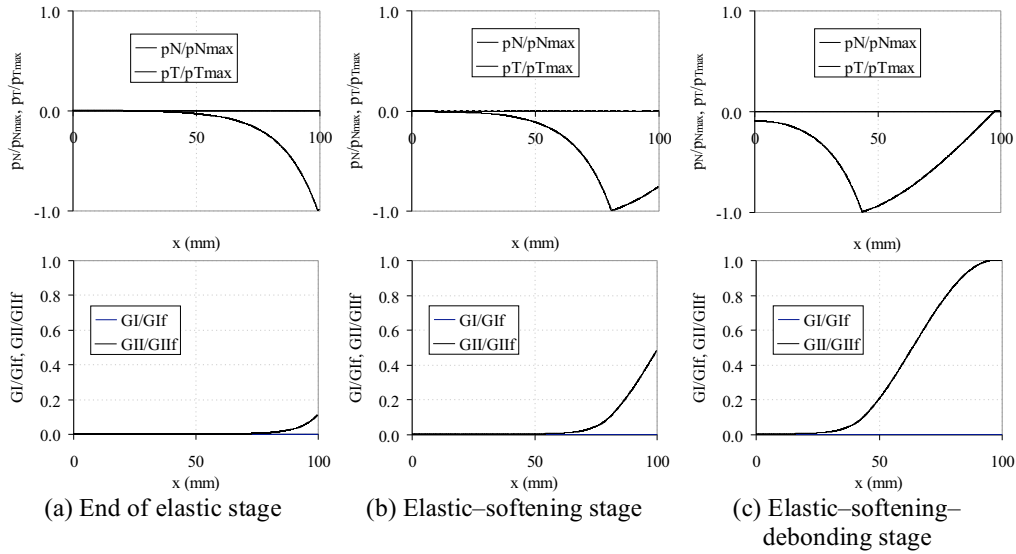


(a) End of elastic stage    (b) Elastic–softening stage    (c) Elastic–softening–debonding stage

Figure 4. Interfacial stresses and energy release rates along the bond length for $\theta = 0°$.

It is interesting to note the variation in mode mixity for the different values of the peel angle. For $\theta = 0°$ (Figure 4) the interface is subjected to tangential stresses and no energy release rate exists in mode I. In this case the peeling load can be predicted by Eq. (2) with $G_f = G_{IIf}$ (Figure 3-b). For $\theta = 10°$ (Figure 6), although the interface is subjected to both normal and tangential stresses, the mode-I energy release rate is largely dominant. Correspondingly, the peeling load can be predicted by Eq. (2) with $G_f = G_{If}$ (Figure 3-b). For $\theta = 2°$ (Figure 5), mode-I and mode-II energy release rates have comparable magnitude. Failure of the element is attained when they reach the boundary of the assumed domain (Eq. 3), as shown by the abrupt drop in interfacial stresses in Figure 5-c. The ratio of $G_{II}$ to $G_I$ at failure in this particular case is equal to 2.28, and the ratio of $G_{II}/G_{IIf}$ to $G_I/G_{If}$ is equal to 0.57. Correspondingly, the numerical value of the peeling load is intermediate between the two solid curves in Figure 3-b.

A final observation is that, as the peel angle increases, the interfacial stress distributions become increasingly localized in the vicinity of the loaded end. This applies to all stages of loading of the interface, thereby generalizing a conclusion drawn by previous researchers at the elastic stage.
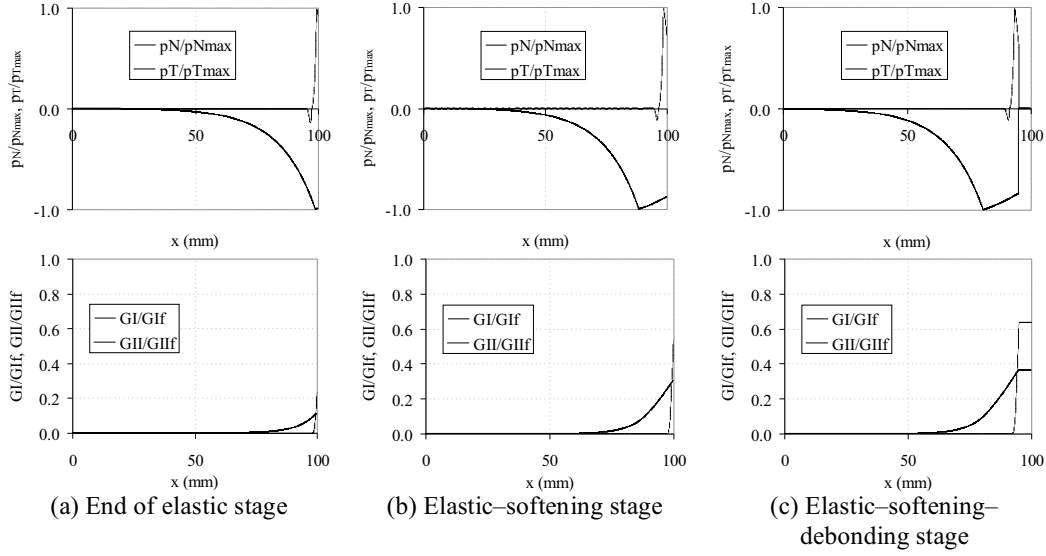
| (a) End of elastic stage | (b) Elastic–softening stage | (c) Elastic–softening– debonding stage |

Figure 5. Interfacial stresses and energy release rates along the bond length for $\theta = 2°$.

### 3.5. Effect of the bond length

It is well known that, for brittle joints under mode-II loading, a value of bond length exists (termed "effective bond length") beyond which a further increase of bond length produces no increase in the debonding load.

Figure 7 illustrates the steady-state peeling force as a function of the bond length, $L$, for three different peel angles. It is evident that the concept of effective bond length can be extended to mixed-mode conditions. Also, the effective bond length is seen to decrease as the peel angle increases, in agreement with the test results by Dai et al. (2004). This is easily explained considering that, as observed earlier, larger peel angles yield a more localized distribution of interfacial stresses. Hence a smaller bond length is needed to "accommodate" the interfacial stress profile corresponding to the full exploitation of the interfacial fracture energies.

### 3.6. Effect of G$_{fII}$/G$_{fI}$

Figure 8 shows the variation of $F_{peel}/p_{T\max}L$ with the peel angle for $G_{IIf}/G_{If} = 1.0$ and $G_{IIf}/G_{If} = 8.0$, as opposed to the value of $G_{IIf}/G_{If} = 4.0$ valid for Figure 3-b. For $G_{IIf}/G_{If} = 1.0$, the fracture energy is mode-independent and Eq. (2) can be used over the full range of peel angles. For $G_{IIf}/G_{If} = 8.0$, once again the numerical results show a gradual transition from the mode-II curve to the mode-I curve as the peel angle increases. Obviously, as $G_{IIf}/G_{If}$ increases, the distance between the two solid curves increases, and hence a more

marked variation of the peel force with the peel angle is observed in the range of peel angles where the transition occurs from mode-II to mode-I dominance. The range of mode-I dominance does not seem to be appreciably affected.
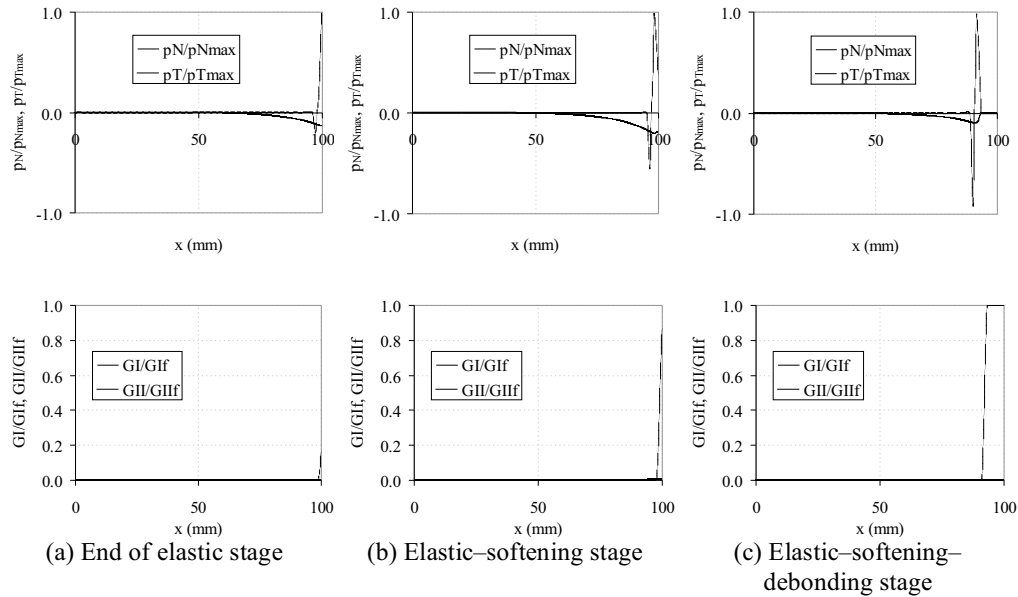


(a) End of elastic stage       (b) Elastic–softening stage       (c) Elastic–softening–
                                                                    debonding stage

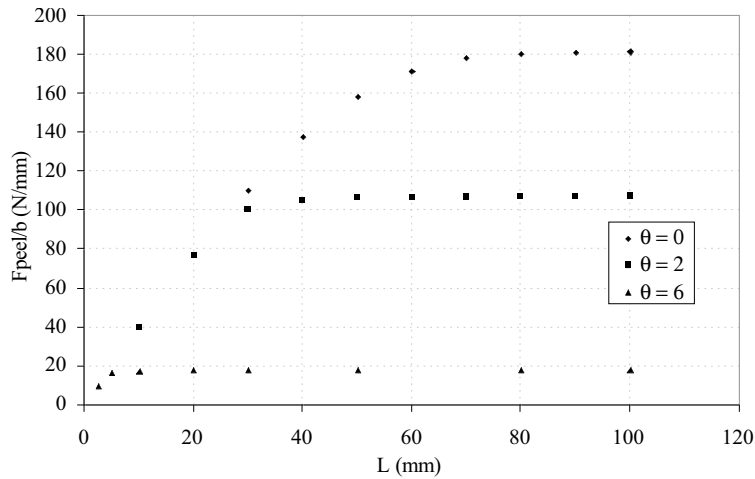Figure 6. Interfacial stresses and energy release rates along the bond length for $\theta = 10°$.



Figure 7. Steady-state peeling force as a function of the bond length for varying peel angles

## 4. CONCLUSIONS

A numerical model of the interface between a quasi-brittle substrate and a thin bonded plate subjected to mixed-mode loading was presented, describing decohesion and contact within a unified framework and using the uncoupled cohesive zone modelling approach allowing for different fracture energies in mode I and mode II. Despite its simplicity, the model appears capable of interpreting various aspects of the physical behaviour effectively, namely the distribution of interfacial stresses and energy release rates along the bond length, and the variation with the peel angle of the debonding load, of the degree of mode mixity and of the effective bond length. Also, the comparison of the numerical results with predictions of Eq. (2) shows that this equation provides upper and lower bounds of the steady-state peeling force.

Developments will involve the study of the remaining variables in Eq. (5), the comparison with test results, the use of other cohesive zone modelling approaches, the consideration of competition between interfacial fracture and crack kinking within the substrate, and the extension to the study of interfacial bond of thin elastic adherends to curved substrates.
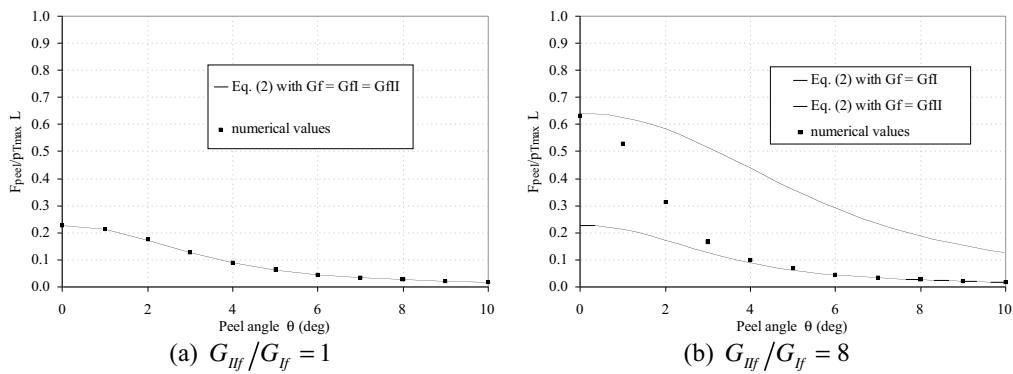


(a) $G_{IIf}/G_{If} = 1$          (b) $G_{IIf}/G_{If} = 8$

Figure 8. Normalized steady-state peeling force as a function of the peel angle.

*References*:

Aravas, N, Kim, K.S., & Loukis, M.J. 1989. On the mechanics of adhesion testing of flexible films. *Materials Science and Engineering*, A107: 159-168.

Bastianini, F. 2003. *Non-destructive techniques for quality assessment and monitoring of bonding in external FRP strengthenings.* PhD thesis, University of Lecce, Italy.

Bikerman, J.J. 1957. Theory of peeling through a Hookean solid. *Journal of Applied Physics*, 28 (12): 1484-485.

Bruno, D., Carpino, R., & Greco, F. 2007. Modelling of mixed-mode debonding in externally FRP reinforced beams. *Composites Science and Technology*, 67: 1459-1474.

Crocombe, A.D., & Adams, R.D. 1982. An Elasto-Plastic Investigation of the Peel Test. *Journal of Adhesion*, 13: 241-267.

Cui, J., Wang, R., Sinclair, A.N., & Spelt, J.K. 2003. A calibrated finite element model of adhesive peeling. *International Journal of Adhesion and Adhesives*, 23: 199-206.

Dai, J.G., Ueda, T., Sato, Y. & Hadiyono, J. 2004. Dowel resistances of bond interfaces between FRP sheets and concrete. *Proceedings of the Second International Conference on FRP Composites in Civil Engineering*, Adelaide, Australia, 371-379.

De Lorenzis, L., Miller, B., & Nanni, A. 2001. Bond of FRP Laminates to Concrete. *ACI Materials Journal*, 98 (3): 256-264.

De Lorenzis, L., Teng, J.G., & Zhang, L. 2006. Elastic interfacial stresses in curved members bonded with a thin plate. *International Journal of Solids and Structures*, 43 (25-26): 7501-7517

Ferracuti, B., Savoia, M., & Mazzotti, C. 2006. A numerical model for FRP-concrete delamination. *Composites: Part B*, 37 (4-5): 356-364.

Högberg, J.L. 2006. Mixed mode cohesive law. *Int. J. of Fracture*, 141: 549-559.

Kafkalidis, M.S., & Thouless, M.D. 2002. The effects of geometry and material properties on the fracture of single lap-shear joints. *Int. J. of Solids and Structures*, 39: 4367-4383.

Karbhari, V.M., Engineer, M., and Eckel II, D.A. 1997. On the durability of composite rehabilitation schemes for concrete: use of a peel test. *J. of Materials Science*, 32: 147-156.

Kim, K.S., & Aravas, N. 1988. Elastoplastic analysis of the peel test. *International Journal of Solids and Structures*, 24 (4): 417-435.

Li, S., Thouless, M.D., Waas, A.M., Schroeder, J.A., & Zavattieri, P.D. 2006. Mixed-mode cohesive-zone models for fracture of an adhesively bonded polymer-matrix composite. *Engineering Fracture Mechanics*, 73: 64-78.

Pan, J., & Leung, C.K.Y. 2007. Debonding along the FRP-concrete interface under combined pulling/peeling effects. *Engineering Fracture Mechanics*, 74: 132-150.

Taljsten, B. 1996. Strengthening of concrete prisms using the plate-bonding technique. *Engineering Fracture Mechanics*, 82: 253-266.

Tvergaard, V. 1990. Effect of fiber debonding in a whisker-reinforced metal. *Materials Science and Engineering*, A125: 203-213.

Van den Bosch, M.J., Schreurs, P.J.G., & Geers, M.G.D. 2006. An improved description of the exponential Xu and Needleman cohesive zone law for mixed-mode decohesion. *Engineering Fracture Mechanics*, 73: 1220-1234.

Wei, Y., & Hutchinson, J.W. 1998. Interface strength, work of adhesion and plasticity in the peel test. *International Journal of Fracture*, 93: 315-333.

Williams, J.G. 1997. Energy release rate for the peeling of flexible membranes and the analysis of blister tests. *International Journal of Fracture*, 87: 265-288.

Wriggers, P., Zavarise, G., & Zohdi, T.I. 1998. A computational study of interfacial debonding damage in fibrous composite materials. *Computational Materials Science*, 12: 39-56.

Xu, X.P., & Needleman, A. 1993. Void nucleation by inclusion debonding in a crystal matrix. Modelling and Simulation and Materials Science and Engineering, 1 (2): 111.132.

Yao, J., Teng, J.G., & Chen, J.F. 2005. Experimental study on FRP-to-concrete bonded joints. *Composites: Part B*, 36: 99-113.

Yuan, H., Teng, J.G., Seracino, R., Wu, Z.S., & Yao, J. 2004. Full-range behaviour of FRP-to-concrete bonded joints. *Engineering Structures*, 26: 553-565.

Yuan, H., Chen, J.F., Teng, J.G., & Lu, X.Z. 2007. Interfacial stress analysis of a thin plate bonded to a rigid substrate and subjected to inclined loading. *International Journal of Solids and Structures*, 44: 5247-5271.